*Technical Physics, 2022, Vol. 67, No. 11*

*06*

# Crystallization and silicon carbide formation in two-layer amorphous silicon-carbon films during electron irradiation

© *A.I. Sidorov,*[1] *E.Ya. Leks,*[2] *O.A. Podsvirov,*[2] *A.Yu. Vinogradov*[3]

[1] ITMO University, St. Petersburg, Russia
[1] Peter the Great Saint-Petersburg Polytechnic University, St. Petersburg, Russia
[3] Ioffe Institute, St. Petersburg, Russia
e-mail: sidorov@oi.ifmo.ru

*Received July 6, 2022*
*Revised August 2, 2022*
*Accepted August 9, 2022*

It is shown that the irradiation by focused electron beam with electron energy of 10 keV of two-layer amorphous silicon-carbon films 60 nm thick results in films partial crystallization. Moreover, in the irradiated zone the layer of crystalline silicon carbide with luminescent properties is formed. The observed effects are confirmed by methods of Raman spectroscopy and by luminescence spectra

**Keywords:** silicon, carbon, silicon carbide, film, structure, electron beam, Raman spectroscopy.

DOI: 10.21883/TP.2022.11.55178.180-22

## Introduction

Carbon and carbon-based materials play an important role in science and technology. This includes, in particular, the study of the properties of amorphous and disordered carbons, as well as the entire spectrum of carbon materials — from graphite and diamond to carbon polymers [1–9]. Amorphous and diamond-like carbon are widely used in a variety of human applications, such as hard magnetic disk coatings, anti-reflective coatings, tribological elements, biomedical coatings, and microelectromechanical systems [6,7]. Graphite and carbon nanotubes are also used in batteries and accumulators [10].

Carbon and silicon and materials based on them, such as silicon carbide, play an important role in science and technology. Silicon-based electronics have revolutionized telecommunications and computer systems [11,12]. Silicon carbide (SiC) is a very attractive material for microelectronics and optoelectronics due to its wide bandgap, high thermal conductivity, excellent thermal and chemical stability and radiation resistance [13]. SiC has more than 170 polytypes [14].

There are many methods for synthesizing films from carbon, silicon and silicon carbide. These include epitaxy [15], magnetron sputtering [16–18], and ion implantation [19]. A number of papers note the influence of synthesis conditions on the structure of the synthesized films. As a rule, the synthesis of these materials in the crystalline phase is carried out at high temperatures.

A focused electron beam with relatively low electron energies (1−10 keV) is a powerful tool for local modification of near-surface layers of materials. Exposure to electrons leads to the breaking of chemical bonds of the material, ionization of material components, and may be accompanied by structural changes in the material. During irradiation, electrons lose energy in the near-surface layer of the target, and the thermally charged electrons create a negatively charged area on the surface and in the near-surface layer of dielectric targets [20,21]. This leads to the field migration of mobile positive ions into the negatively charged area, which causes a local change in the chemical composition of the material [22,23]. This process may be accompanied by local crystallization of amorphous and glassy materials [24,25].

The effects of electrons on materials are very diverse. Electron beam effect allows the formation of metallic nanoparticles in metal-containing crystals and glasses [24–27] as well as the formation of luminescent centers [27]. Effect to electrons can lead to the transformation of the amorphous phase into a crystalline one in such materials as $ZrO_2$, $TiO_2$, silicon, some alloys such as Fe−C, etc. [28–35]. The advantage of electron-beam modification of materials is that the electron beam can be focused into a spot of less than 10 nm in diameter. This makes it possible to modify the properties of materials on the nanoscale.

The aim of this work was to study the structural changes in bilayer amorphous silicon-carbon thin films when irradiated by electrons with an energy of 10 keV. Structural changes in amorphous silicon and carbon thin films are shown, and a new method of synthesis of silicon carbide that takes place at low temperatures is proposed.

## 1. Materials and methods

Two-layer silicon-carbon films on silicate glass substrates produced by magnetron sputtering were used in the experiments. The thickness of each film was 30 nm. Two groups of samples were prepared. In the I group, the silicon film was deposited on the carbon film. In II group of samples, the carbon film was deposited on the silicon

film. Amorphous films of carbon and silicon were prepared by magnetron sputtering at constant current of carbon and silicon targets in an argon discharge. The substrates were heated only by plasma radiation from 20°C at the beginning of the film deposition to 80°C at the end of the process. It is known that film crystallization does not occur at these temperatures. Before the films were applied, sputtering modes were determined to obtain the desired film thickness. The argon pressure in the chamber during sputtering was 0.01 Pa, the sputtering time — 15 min.

The samples were electron irradiated using a JEBD-2 scanning electron microscope (JEOL) at room temperature. The energy of the electrons was 10 keV. The electron current density in the focused beam was $30\,\mu$A/cm$^2$ and the electron dose — 30 mC/cm$^2$. The diameter of the electron beam on the surface of the samples was 1 mm for convenient optical measurements. The irradiation was performed at a pressure of $10^{-5}$ Pa in the chamber.

Raman spectra were measured using an inVia Raman microscope (Renishaw) with arbitrary polarization and an excitation wavelength of 633 nm. Measurements were taken not only in the irradiated area of the film, but also on the glass surface. It was found that the Raman bands of the glass do not overlap the Raman bands of the film (see below), and therefore do not affect the measurement results. Luminescence spectra were measured with an LS-55 spectro-fluorimeter (Perkin Elmer) at an excitation wavelength of 310 nm. Spectral measurements were performed at room temperature.

## 2. Results and discussion

Experiments have shown that the results for I and II groups of samples are approximately the same, only the intensities of Raman peaks differ, so below, we will present results only for group I of samples. After electron irradiation, the irradiated areas of the samples become darker compared to the surrounding ones. Figure 1, *a* shows the Raman spectrum of an unirradiated silicon-carbon film. The figure shows that the most intense band consists of two overlapping bands with maxima at 1350 and 1500 cm$^{-1}$. The first peak ($D1$) corresponds to the breathing mode $A_{1g}$ of amorphous carbon. This mode is forbidden in crystalline graphite and appears only in amorphous carbon and in disordered graphite [36,37]. The second peak ($G$) refers to the bond stretching mode between a pair of $sp^2$-atoms of carbon. This mode has symmetry $E_{2g}$. In ideal crystalline graphite, the maximum of this peak occurs at a frequency of 1581 cm$^{-1}$. As the disorder in carbon increases, this peak shifts to lower frequencies [36]. Other intense peaks refer to the glass substrate. According to [35–37], the band with a maximum at $\nu = 1075$ cm$^{-1}$ corresponds to the Si−NBO (NBO — nonbridging oxygen) stretching mode. The band near $\nu = 800$ cm$^{-1}$ refers to the symmetric tensile modes in the anionic structural unit $(SiO_4)^{4-}$. The band with a maximum at $\nu = 600$ cm$^{-1}$ corresponds to the symmetric breathing oscillations of oxygen in four- and three-linked siloxane rings composed of $SiO_4$ tetrahedrons. The band near 465 cm$^{-1}$ can be attributed to bond vibrations in Si−O−Si in 4−6-linked siloxane rings.

Fig. 1, *b* shows the Raman band in the frequency range 1100−1800 cm$^{-1}$ before and after electron irradiation. The figure shows that after electron irradiation, the band becomes more structured, and the peaks become narrower. Peak $G$ shifts to the region of higher frequencies. This indicates a decrease in the disorder in the carbon film. In addition, a peak appears at $\nu = 1620$ cm$^{-1}$.

Fig. 1, *c* shows the Gaussian decomposition of the *2* curve from Fig. 1, *b*. The figure shows that the Raman band consists of 5 peaks. Three $D3$ peaks at frequencies 1460, 1520 and 1550 cm$^{-1}$ are caused by vibrations in disordered graphite [7,32,33]. The $G$-peak is shifted by $\nu = 1580$ cm$^{-1}$. This indicates the appearance of graphite-like structures.The $D2$-peak at $\nu = 1620$ cm$^{-1}$ characterizes oscillations on the surface of the graphite film. The figure also shows that the $D$-peak at $\nu = 1350$ cm$^{-1}$, caused by breathing modes in amorphous carbon, disappears. Thus, electron irradiation leads to partial crystallization of amorphous carbon into graphite-like structures.

Figure 1, *d, e* shows the Raman spectra of the silicon-carbon film in the 450−650 and 260−340 cm$^{-1}$ frequency ranges before and after electron irradiation. The figure shows that electron irradiation leads to the appearance of Raman bands at frequencies near 550 and 305 cm$^{-1}$. The first band is responsible for vibrations in the transverse optical mode of crystalline silicon. The second band can be correlated with the second-order transverse acoustic mode of crystalline silicon [38]. Both bands are broadened due to the disordered structure of crystalline silicon. Thus, electron irradiation leads to partial crystallization of amorphous silicon.

Experiments have shown that electron irradiation leads to the appearance of bright yellow luminescence in the irradiated area (inset in Fig. 2). The luminescence spectra are shown in Fig. 2. The figure shows, that there are two bands in the luminescence spectrum: an intense and narrow luminescence band with a maximum at 380 nm and a broad luminescence band with a maximum at 550 nm. Such luminescence is characteristic of 4H−SiC and 6H−SiC (hexagonal forms of silicon carbide)The first luminescence band is caused by exciton transitions, the second band - transitions from deep impurity levels in the band gap formed by lattice defects of silicon carbide [39].

Raman spectra in the 700−1000 cm$^{-1}$ frequency range were examined to confirm the formation of silicon carbide under electron irradiation (Fig. 3). The two bands are present before and after electron irradiation. The decomposition into Gaussians in Fig. 3 corresponds to the blue curves (in online version). They refer to symmetrical tensile modes in the anionic structural unit $(SiO_4)^{4-}$ silicate glass [40–42]. Electron irradiation results in two broad bands at frequencies 790 and 900 cm$^{-1}$. The first band corresponds to the transverse optical 6H−SiC mode, the

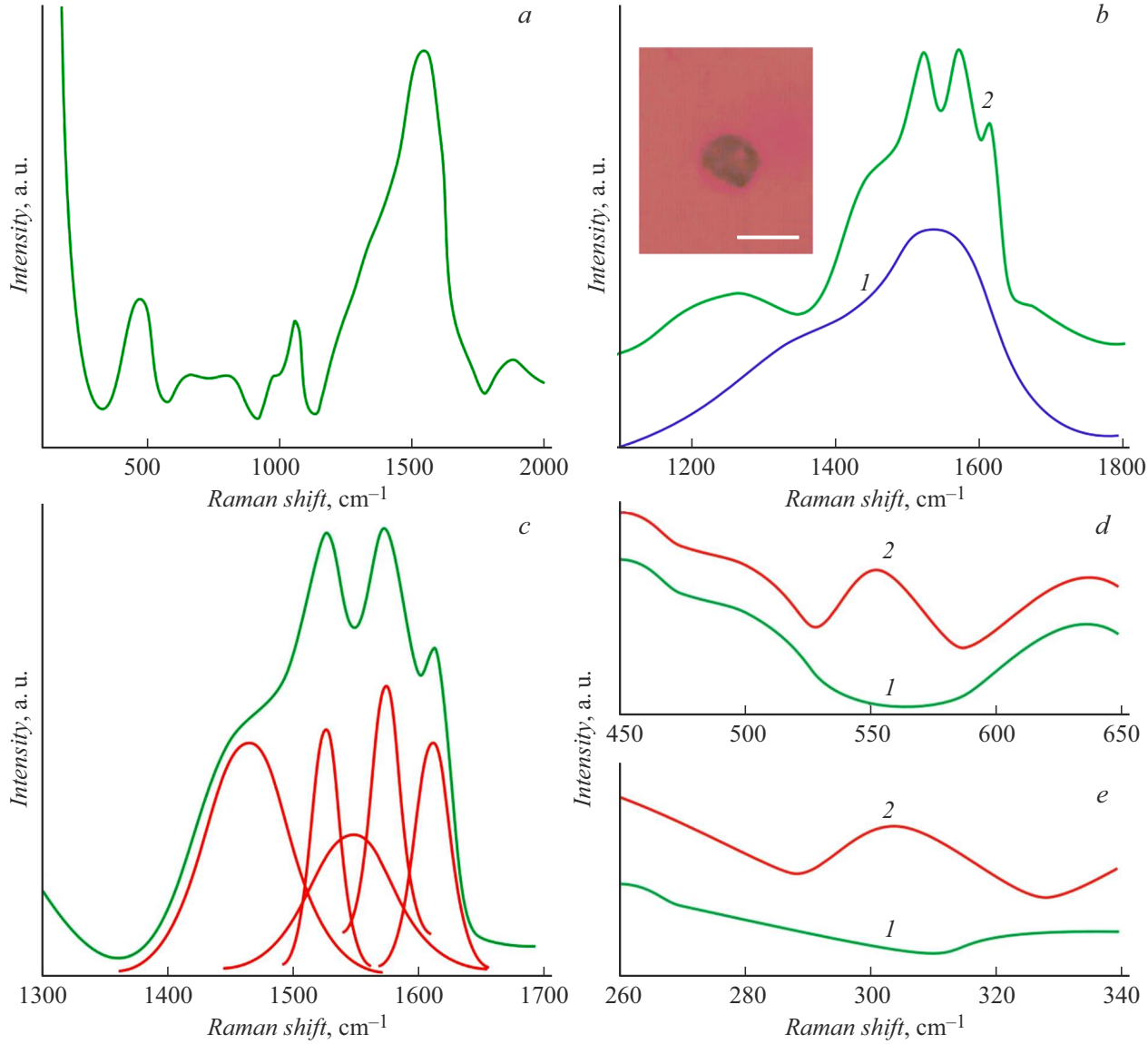


**Figure 1.** Raman spectra of silicon-carbon film on silicate glass substrate: *a* — general view of the Raman spectrum of the unirradiated film; *b, d, e–1* — before irradiation, *2* — after irradiation; *c* — decomposition into Gaussian curve *2* in Fig. 1, *b*. Insert — image of the irradiated area. The scale is 2 mm.

second band — the longitudinal optical 6H−SiC [43,44] mode. The band broadening is due to the formation of structural defects during electron irradiation. In addition, electron irradiation can lead to the formation of other SiC polytypes that have bands in this frequency area. For example, 4H−SiC, 2H−SiC, 15R−SiC [45]. Thus, electron irradiation of a bilayer silicon-carbon film leads to the formation of crystalline silicon carbide in the irradiated zone.

Numerical simulations showed that the temperature of the near-surface layer of glass during electron irradiation with 10 keV energy does not exceed 120°C. Electrons with this energy have almost no energy loss in a silicon-carbon film 60 nm thick. A Monte Carlo simulation showed that the maximum energy loss of electrons lies below the glass surface at a depth of about 200 nm (Fig. 4).

Thus, thermal processes and the direct effect of primary electrons cannot influence the crystallization processes in the film. In the electron irradiation process, secondary electrons are emitted mainly from the substrate. Secondary electron emission consists of elastically and inelastically scattered electrons and the actual secondary electron emission [46]. The total secondary electron emission coefficient for a primary electron energy of 0.5−10 keV in quartz glass reaches 4 [46]. The maximum yield depth of the proper secondary electrons does not exceed 10 nm. The energy of the secondary electrons is in the range of a few tens of electron-volts [46]. Therefore, the effect of secondary electrons escaping from the glass into the silicon-carbon film is similar to the effect of laser radiation, which can also lead to crystallization of amorphous materials. Secondary

electrons with the above energies break the covalent bonds present in amorphous silicon and carbon. This causes a change in the atomic cluster structure in the amorphous state. The result is a change in the equilibrium state of atoms near a pair of atoms with broken chemical bonds. After such changes in the position of the atoms, a new atomic structure can be formed. And it can be similar to the structural unit of a crystal lattice. Transformation of the amorphous phase into a crystalline phase in this case is possible because the crystalline state has less potential energy than the amorphous state. Similar process leads to the formation of silicon carbide at the boundary between the silicon and carbon films. Thus, electron irradiation of the silicon-carbon film compared to traditional methods allows the synthesis of silicon carbide at a very low temperature. For example, in [15] the SiC film was grown by epitaxy at 1100−1350°C, in [19] the SiC film was formed by ion-beam deposition at 700−1220°C.

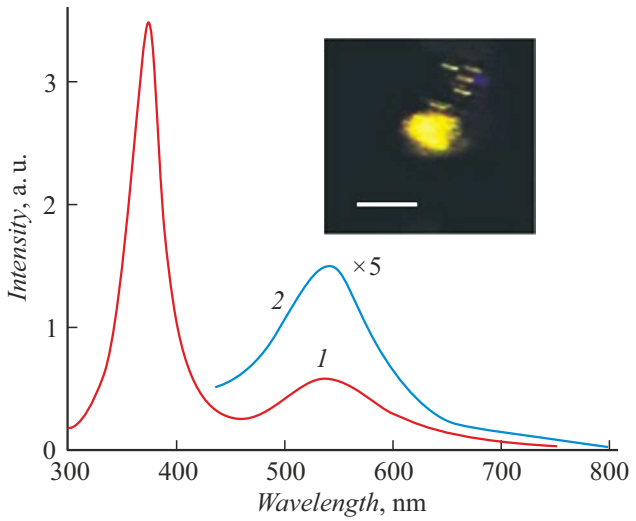


**Figure 2.** Luminescence spectra of silicon-carbon film after electron irradiation. Excitation wavelength: *1* — 300, *2* — 390 nm. Insert: photo of luminescence in the irradiated area. The scale is 1 mm.

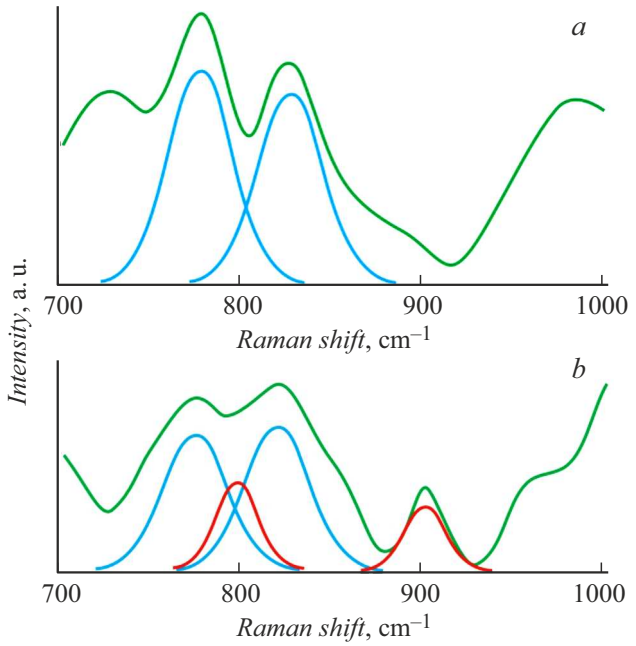


**Figure 3.** Raman spectra of the silicon-carbon film in the spectral range 700−1000 $cm^{-1}$ and their decomposition into Gaussians (blue and red curves (online version)). *a* — before electron irradiation, *b* — after electron irradiation.

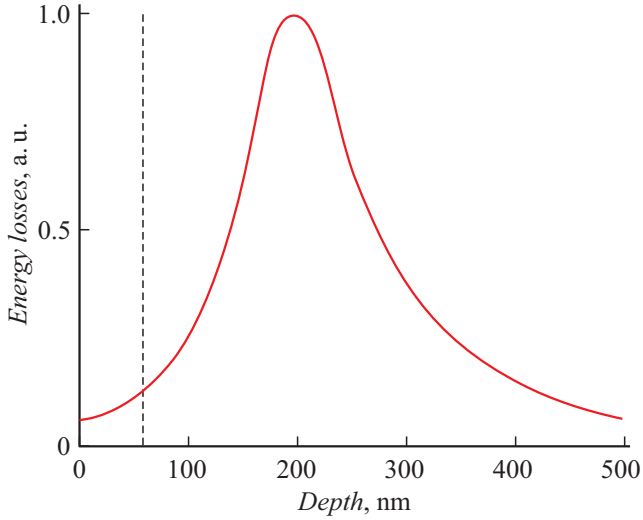


**Figure 4.** Calculated distribution of electron energy losses in silicate glass with bilayer silicon-carbon film. The energy of the electrons is 10 keV. Stroke — the boundary between the film and the glass.

## Conclusion

Experiments have shown that electron irradiation of thin bilayer amorphous silicon-carbon films leads to partial crystallization of the films. At the boundary between silicon and carbon, crystalline silicon carbide of hexagonal shape is formed, mainly 6H−SiC. The main contribution to these processes is made by secondary electrons that break chemical bonds in amorphous silicon and carbon, which allows the formation of new structural units characteristic of crystalline silicon and carbon, as well as silicon carbide.

### Financial support of work

This study was performed as part of the Program „Priority 2030“.

### Conflict of interest

The authors declare that they have no conflict of interest.

## References

[1] C. Casiraghi, J. Robertson, A.C. Ferrari. Mater. Today, **10**, 44 (2007).
[2] R. Hauert. Tribol. Int., **37**, 991 (2004).
[3] J.P. Sullivan, T.A. Friedmann, K. Hjort. MRS Bull., **26**, 309 (2001).
[4] A.C. Ferrari. Surf. Coat. Technol., **180**−181, 190 (2004).
[5] A.C. Ferrari, J. Robertson. Phys. Rev. B, **61**, 14095 (2000).
[6] A.C. Ferrari, J. Robertson. Phys. Rev. B, **64**, 075414 (2001).
[7] C. Casiraghi, A.C. Ferrari, J. Robertson. Phys. Rev. B, **72**, 085401 (2005).
[8] A.C. Ferrari, S.E. Rodil, J. Robertson. Phys. Rev. B, **67**, 155306 (2003).
[9] B. Racine, A.C. Ferrari, N.A. Morrison, I. Hutchings, W.I. Milne, J. Robertson. J. Appl. Phys., **90**, 5002 (2001).
[10] A.C. Ferrari, J. Robertson. Philos. Trans. R. Soc. Ser. A, **362**, 2267 (2004).
[11] P.B. Griffin, J.D. Plummer, M.D. Deal. *Silicon VLSI Technology: Fundamentals, Practice, and Modeling* (Prentice Hall, NY., 2000)
[12] H.S. Nalwa (ed.). *Silicon Based Materials and Devices* (Academic Press, NY., 2001)
[13] O. Kordina, L.O. Bjorketun, A. Herry, C. Hallin, R.C. Glass, L. Hultman, J.E. Sundgren, E. Janzen. J. Cryst. Growth, **154**, 303 (1995).
[14] M.J. Pelletier. *Analytical Applications of Raman Spectroscopy* (Blackwell Science, UK, 1999)
[15] T.S. Perova, J. Wasyluk, S. A. Kukushkin, A.V. Osipov, N.A. Feoktistov, S.A. Grudinkin. Nanoscale Res. Lett., **5**, 1507 (2010). DOI: 10.1007/s11671-010-9670-6
[16] Y. Cheng, X. Huang, Z. Du, J. Xiao. Opt. Mater., **73**, 723 (2017).
[17] W. Yizhe, T. Zha-ma, Y. Zhenming, S. Hui, G. Jianhong, J. Gao. Chin. J. Phys., **64**, 79 (2020). https://doi.org/10.1016/j.cjph.2020.01.006
[18] M. Qi, J. Xiao, Y. Cheng, Z. Wang, A. Jiang, Y. Guo, Z. Tao. AIP Adv., **7**, 085012 (2017).
[19] I.V. Mirgorodskiy, L.A. Golovan, V.Yu. Timoshenko, A.V. Semenov, V.M. Puzikov. Semiconductors, **48** (6), 711 (2014). https://doi.org/10.1134/S1063782614060207
[20] M. Touzin, D. Goeriot, C. Guerret-Piecort, D. Juve, D. Treheux, H.-J. Fitting. J. Appl. Phys., **99**, 114110 (2006).
[21] A.I. Ignatiev, A.V. Naschekin, D.M. Nevedomsky, O.A. Podsvirov, A.I. Sidorov, A.P. Soloviev, O.A. Usov. Techn. Phys., **56** (5), 662 (2011). https://doi.org/10.1134/S1063784211050148
[22] N. Jiang, J. Qiu, J.C.H. Spence. Appl. Phys. Lett., **86**, 143112 (2005).
[23] O.A. Podsvirov, A.I. Sidorov, D.V. Churaev. Tech. Phys., **59** (11), 1674 (2014). https://doi.org/10.1134/S1063784214110218
[24] A.V. Vostokov, I.A. Verzin, A.I. Ignat'ev, O.A. Podsvirov, A.I. Sidorov. Opt. Spectr., **109** (3), 366 (2010).
[25] E.S. Bochkareva, N.V. Nikonorov, O.A. Podsvirov, M.A. Prosnikov, A.I. Sidorov, Plasmonics, **11**, 241 (2016).
[26] E.S. Bochkareva, A.I. Sidorov, U.V. Yurina, O.A. Podsvirov. Nucl. Instr. Meth. Phys. Res. B, **403**, 1 (2017).
[27] E.A. Ilina, A.I. Sidorov, U.V. Yurina, O.A. Podsvirov. Nucl. Instr. Meth. Phys. Res. B, **412**, 28 (2017).
[28] A.G. Bagmut, V.M. Beresnev. Phys. Sol. State., **59**, 151 (2017).
[29] S.R. Nitul, S.-G. Kim, J.B. Chou, J. Abed, J. Viegas, M. Jouiad. MRS Adv., **1**, 825 (2015).
[30] T. Bret, T. Hofmann, K. Edinger. Appl. Phys. A, **117**, 1607 (2014).
[31] A. Botman, J.J.L. Mulders, C.W. Hagen. Nanotechnol., **20**, 372001 (2009).
[32] S.M. Zharkov, L.I. Kveglis, Phys. Sol. Stat., **46**, 969 (2004).
[33] J. Shim, J.A. Rivera, R. Bashir. Nanoscale, **5**, 10887 (2013).
[34] N. Jianga B. Wu, J. Qiu, J.C.H. Spence. Appl. Phys. Lett., **90**, 161909 (2007).
[35] A.I. Sidorov, N.S. Zaitsev, O.A. Podsvirov. Phys. B: Cond. Mat., **598**, 412439 (2020).
[36] A. Sadezky, H. Muchkenhuber, H. Grothe, R. Niessner, U. Pöschl. Carbon, **43**, 1731 (2005).
[37] S. Karekin, D. Esmeryan, E.C. Castano, H.A. Bressler, M. Abolghasemibizaki, P.C. Fergusson, A. Roberts, R. Mohammadi. Diamond Related Mater, **75**, 58 (2017).
[38] S. Piscanec, A.C. Ferrari, M. Cantoro, S. Hofmann, J.A. Zapien, Y. Lifshitz, S.T. Lee, J. Robertson. Mater. Sci. Eng. C, **23**, 931 (2003).
[39] I.G. Aksyanov, I.V. Kul'kova, S.A. Kukushkin, A.V. Osipov, N.A. Feoktistov, M.E. Kompana. Phys. Sol. State, **51**, 2469 (2009).
[40] G. Pacchioni, L. Skuja, D.L. Griscom (ed.). *Defects in $SiO_2$ and Related Dielectrics: Science and Technology* (Springer Dordrecht, 2000), v. 2.
[41] A. Quaranta, A. Rahman, G. Mariotto, C. Maurizio, E. Trave, F. Gonella, E. Cattaruzza, E. Gibaudo, J.E. Broquin. J. Phys. Chem. C, **116**, 3757 (2012).
[42] A. Osipov, L. Osipova, R. Zainullina. Int. J. Spectrosc. **2015**, 572840 (2015).
[43] J. Wasyluk, T.S. Perova, S.A. Kukushkin, A.V. Osipov, N.A. Feoktistov, S.A. Grudinkin, Mater. Sci. Forum, **359**−**362**, 645 (2010).
[44] R.V. Konakova, O.F. Kolomys, O. Okhrimenko, V.V. Strelchuk, E.Yu. Volkov, M.N. Grigoriev, A.M. Svetlichnyi, O.B. Spiridonov. Semiconductors, **47** (6), 812 (2013).
[45] S. Nakashima, H. Harima. Phys. Stat. Sol. A, **162**, 39 (1997).
[46] H. Semat, J.R. Albright. *Introduction to Atomic and Nuclear Physics* (Chapman and Hall, London, 1972)